ADVANCED FUNCTIONAL MATERIALS
www.afm-journal.de

Materials Views
www.MaterialsViews.com

Giant Temperature Coefficient of Resistance in Carbon Nanotube/Phase-Change Polymer Nanocomposites

Gustavo E. Fernandes, Jin Ho Kim, Ashok K. Sood, and Jimmy Xu*

The temperature coefficient of resistance of a carbon nanotube nanocomposite with the non-conductive phase-change hydrogel Poly(N-isopropylacrylamide) is studied. This nanocomposite is found to achieve the largest reported temperature coefficient of resistance, ≈−10%/°C, observed in carbon nanotube-polymer nanocomposites to date. The giant temperature coefficients of resistance results from a volume-phase-transition that is induced by the humidity present in the surrounding atmosphere and that enhances the temperature dependence of the resistivity via direct changes in the tunneling resistance that electrons experience in moving between nearby carbon nanotubes. The bolometric photoresponses of this new material are also studied. The nanocomposite's enhanced responses to temperature and humidity give it great potential for sensor applications and uncooled infrared detection.

1. Introduction

Carbon nanotube (CNT) nanocomposites have attracted considerable attention in recent years because of their potential applications in electronics and sensing.[1] Electromagnetic radiation sensing via bolometeric operation[2] is one emerging application for these materials.[3,4–6] Bolometers operate via thermotransduction–electromagnetic radiation is absorbed and converted into heat, which in turn changes the bolometer material's electrical resistivity according to the temperature coefficient of resistance (TCR). It has been shown that the responses of thin CNT films to electromagnetic radiation is dominated by bolometric effects.[7] Thin membranes of CNTs and CNT nanocomposites with polymers and other materials have much to offer in terms of bolometric sensing.[4] They display strong and broad-band absorbance, which enables detection over broad ranges of the electromagnetic spectrum.[8] Their electrical and thermal conductivities can be tailored by appropriate selection of CNT chirality (semiconducting, metallic, or ratios thereof), type (single walled or multi-walled), doping and structure (e.g., crystalline vs. polycrystalline).[9] In addition, CNT membranes are known to have large strength-to-weight ratios,[10] which may facilitate the fabrication of robust standalone suspended structures that are required for heightened heat sensitivity. CNTs are also chemically inert to a large variety of chemical species.[11] Currently, reported TCR values for CNT membranes and nanocomposites are in the neighborhood of −0.5%/ °C near room temperature,[3,4,12] while infrared responsivities as large as 500 V/W have been reported.[7] These figures still compare unfavorably with those for vanadium oxide, the leading platform for uncooled bolometric detection, in which TCR values in excess of 3%/ °C[13] and responsivities in the tens of MV/W have been observed.[14]

$$\sigma = \sigma_0 e^{-(T_0/T)^{\alpha}} \tag{1}$$

The electrical resistance of a membrane of randomly dispersed CNTs is known to be dominated by the tunneling of electrons between nearby CNTs.[15] This type of electrical transport is commonly described in the framework of the variable range hopping VRH model,[16,17–20] according to which the conductivity of a CNT membrane is given by Equation (1), where T_0 is an activation energy (in units of temperature), T is the temperature, and α is given by $1/(d+1)$, where d is the dimensionality that characterizes transport (e.g., $\alpha = 1/4$ in three dimensions, 1/3 in two dimensions and 1/2 in one dimension).[19] T_0 contains information about the tunneling process,[20] including the mean CNT-CNT tunneling barrier height and width, and the mean contact area. T_0 also contains, via the permittivity, information about the properties of the non-conductive medium that fills the space between CNTs, as will be discussed in more detail later. A general expression for the TCR can be easily derived from Equation 1, and is given by

$$TCR = \frac{\alpha}{T^2}\left(\frac{T_0}{T}\right)^{\alpha-1}\left(TT_0' - T_0\right) \tag{2}$$

where T'_0 is the derivative of T_0 with respect to T. It is clear from Equation (2) that the TCR, having terms proportional to both T_0 and T'_0, could be enhanced via nanoengineering of these two parameters. One way to accomplish such a task is via incorporation of non-conductive polymers into the CNT film. Polymers having strongly temperature dependent properties, such as large thermal expansion coefficient or large temperature dependence of the permittivity could be particularly good candidates. In addition, polymers that experience

Dr. G. E. Fernandes, Dr. J. H. Kim, Prof. J. Xu
Brown University
School of Engineering
Providence, RI 02912, USA
E-mail: gustavo_fernandes@brown.edu
Dr. A. K. Sood
Magnolia Optical Technologies Inc.
52-B Cummings Park, Woburn, MA 01801, USA

DOI: 10.1002/adfm.201300208

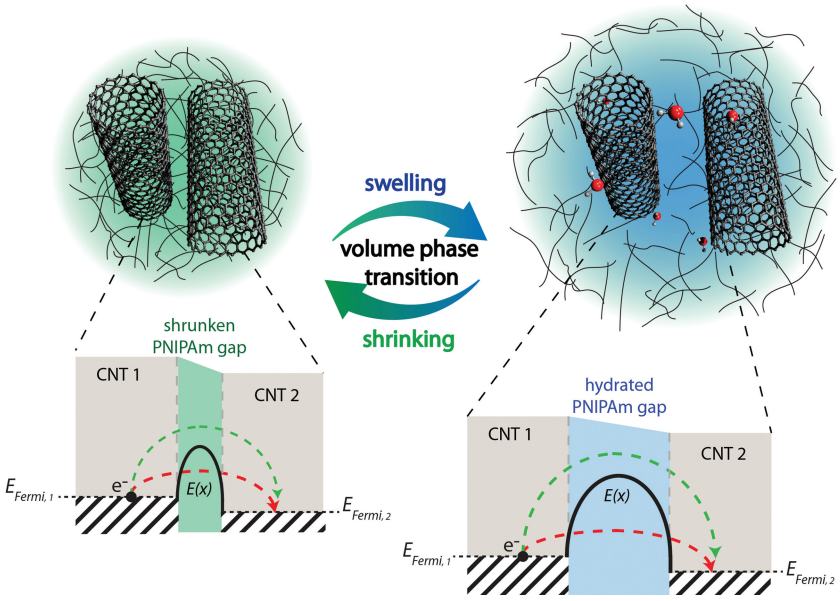

Figure 1. Illustration of the effects of volume phase change on the intertube spacing in and the intertube electron tunneling potential barrier. As the nanocomposite absorbs moisture at low temperatures and becomes hydrated the resulting VPT increases both the intertube distances and the tunneling potential barrier heights. Because the volume phase change is reversible, the intertube distances and potential barriers are restored when the temperature is increased.

phase transitions or glass transitions could be good candidates because enhanced temperature dependences in many material parameters are expected near the transition temperature.

In this article we investigate the enhancement of the TCR in a CNT membrane via the incorporation of a non-conducting phase-change polymer, Poly(N-isopropylacrylamide) (PNIPAm).[21,22] PNIPAm is known to experience a volume phase transition (VPT) that depends upon both temperature and humidity conditions, and results in remarkable changes in the volume and in the permittivity.[23] This reversible transition dynamically changes the CNT-to-CNT contact properties, as illustrated in **Figure 1**. In our study, the CNT-PNIPAm nanocomposites experienced large changes in conductivity near the VPT critical temperature, leading to TCR several times greater than those observed in previous studies of CNT-polymer composites.

2. Results and Discussions

2.1. Temperature Dependence of Resistance and TCR

As seen in **Figure 2**, large changes in the resistance were observed as the nanocomposite temperature approached the dew point temperature. The dew point temperature corresponds to the temperature at which condensation begins to occur on the sample surface. At the dew point temperature, a significantly larger supply of moisture becomes available, and incorporation of water (and the accompanying volume expansion of the nanocomposite) resulted in TCR values about one order of magnitude greater than previous observations in CNT-polymer composites.[3,4,6] The sample in Figure 2 showed maximum TCR ≈–10%/ °C. However, TCR as large as –40%/ °C were achieved in other samples consisting of higher resistance films. Similar CNT films without PNIPAm were also tested but did not show appreciable changes in the resistance and their TCR remained below ≈–0.8%/ °C through the entire measured temperature range. Additionally, measurements of the nanocomposite samples at 0% relative humidity revealed no signature of the VPT in the TCR versus temperature curves, as shown in Figure 2a.

The temperature dependence of the electrical conductivity, shown in Figure 2b, suggests two distinct ranges of constant T_0 (i.e., constant slope in the graph of Figure 2b) connected by a transition region. We have labeled these the high temperature (HT) and the low temperature (LT) regions. The transition region between the HT and LT regions can be identified with the VPT, as discussed below. In this region hydration/dehydration, as well as the resulting swelling/shrinking of the nanocomposite, gives rise to dynamically changing conductivity as a function of temperature. The value 1/2 was chosen for the VRH parameter α in Equation 1 (and in the temperature axis of Figure 2b) because it consistently gave slightly better linear fits for all values of the relative humidity tested. The curvature of the logarithmic resistance curves in the transition region in Figure 2b indicates that T_0 depends on the temperature in this region. The transition region was observed to encompass a window of temperatures a few degrees wide and centered at the dew point temperature for each value of the relative humidity.

PNIPAm's hydrophobic-to-hydrophilic phase transition is known to occur near 32 °C, which is higher than the temperatures at which the transition regions were observed in Figure 2b. This suggests that the transition region does not result directly from the hydrophobic-to-hydrophilic phase transition, but may instead be related to the VPT. In our experimental setup, these two transitions, hydrophobic-to-hydrophilic and VPT, are decoupled via the control of the relative humidity. The VPT occurs only in the presence of moisture and, in a humid atmosphere, the availability of moisture is determined both by the atmospheric temperature and the relative humidity. Previous studies[21,24] on PNIPAm have considered the VPT in aqueous (fully saturated) media. The unlimited supply of moisture in such cases causes the VPT to occur simultaneously with the hydrophobic-to-hydrophilic transition. In our experimental setup, however, the supply of moisture only approximates the fully hydrated condition when the temperature is lower than the dew point temperature.

The VRH model with $\alpha = 1/2$ is known to arise for systems in which charge accumulation in the isolated conductive particles (CNTs) leads to a Coulomb-force contribution to the tunneling process. This model predicts[17,20]

$$T_0 = (128\pi^2 m^* \theta / k_B^2 h^2)^{1/2} s\, E_c^0 \quad (3)$$

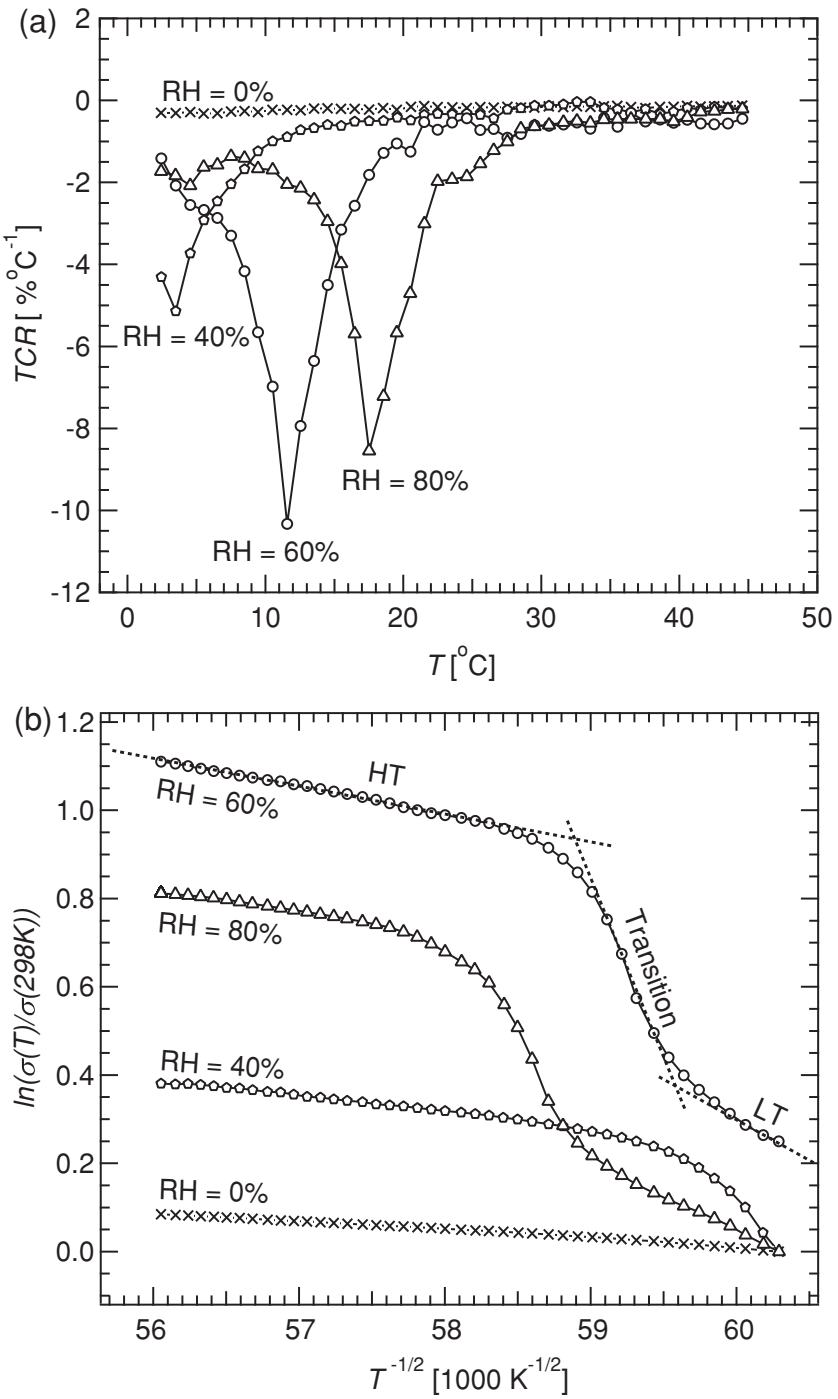

Figure 2. Enhanced TCR and conductivity response via volume phase change. a) Temperature behavior of the TCR at various relative humidity levels. The point of largest TCR occurs at the volume phase change temperature, which in our setup corresponds to the dew point of water. b) Temperature behavior of the conductivity (normalized to the value at 45 °C at various relative humidity levels. The curve corresponding to 60% relative humidity is offset vertically for better viewing. The dashed lines serve as a guide to the eye in identifying the different regions discussed in the text. The thickness of the film is ≈500 nm.

where $m*$ is the electron effective mass in the CNT, θ is the mean barrier height of the CNT-PNIPAm-CNT contact, h is Planck's constant, s is the mean separation distance between CNTs, and $E^0_c = 2e^2/\varepsilon_i d$ is the charging energy that depends on the relative permittivity ε_i of the insulating medium (PNIPAm) and the average diameter d of the conductive nanoparticles. Equation 3 assumes spherical nanoparticles,[20] which represents a significant deviation from the elongated and tubular CNT geometry. Therefore we use it here simply to obtain a qualitative understanding of the effects of the VPT on the parameters affecting T_0.

Most of the parameters appearing in Equation 3 can be affected by the VPT. The CNT-CNT separation and tunneling barrier height (s and θ) are expected to increase as the polymer hydrates and expands (and to decrease as the polymer dehydrates and contracts). The relative dielectric permittivity of PNIPAm (ε_i) is found to strongly depend on the temperature. It decreases from ≈63 at 15 °C to ≈17 at 40 °C[25] and is affected by hydration/dehydration, as well as the volume expansion/contraction of the nanocomposite.[18] The parameters d and $m*$, which pertain only to the CNTs, are not expected to change directly with the VPT, but could be affected by strains[26] or by varying surface passivation conditions that may result from the VPT.

2.2. Bolometric Photoresponse

The enhancement in the TCR observed in these nanocomposites can be expected to lead to an enhancement in the bolometric responsivity. However, a few caveats must be discussed with regards to this expected enhancement. Firstly, the hydration/dehyration of the nanocomposite in the VPT region is expected to change the nanocomposite's thermal properties, namely the heat capacity (C_{Th}) and the thermal conductivity (thus the thermal resistance R_{Th} that couples the bolometer to its surroundings). These are expected to manifest as an increase in the thermal time constant ($\tau = R_{Th}C_{Th}$) of the bolometer and will affect the response time. Secondly, the bolometer's responsivity ($\Re$) is given by[2]:

$$\Re = \frac{\eta i_b R\beta R_{Th}}{(1+\tau^2\omega^2)^{1/2}} \quad (4)$$

where η is the optical absorption, i_b is the electrical bias current, β is the TCR, R is the bolometer electrical resistance (at the operating point), and ω is the angular frequency of signal modulation. Equation 4 suggests that the maximum expected enhancement in the responsivity corresponds to the product $R\beta$, all other factors remaining unchanged. Finally, from the TCR curves shown in Figure 2a, the system response

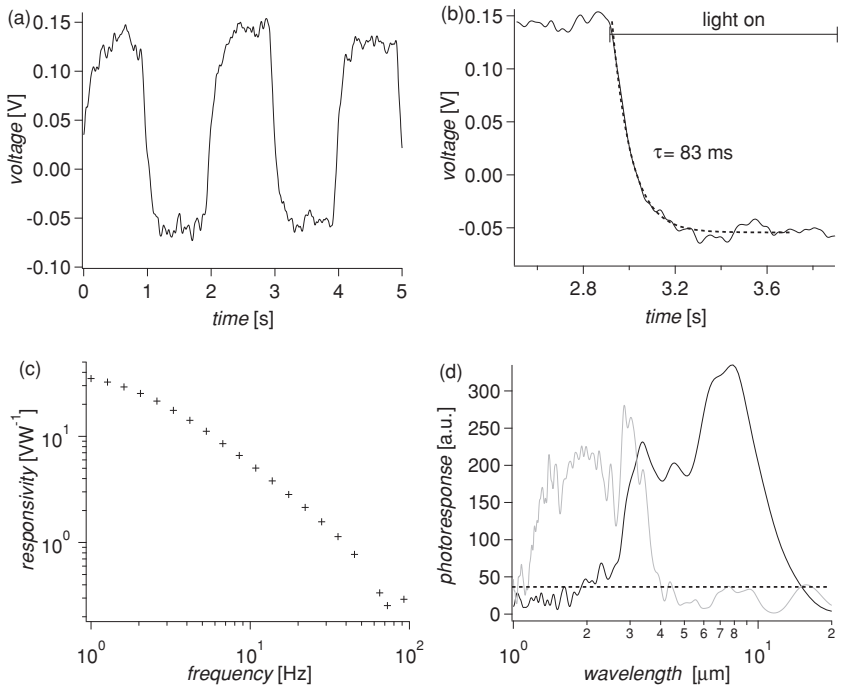

Figure 3. a) Time dependence of photoresponse for CNT-PNIPAm bolometer measured at 60% relative humidity and 19 °C. b) Close up of (a) showing an exponential decay fit to the bolometer signal as the illumination is turned on. c) Modulation frequency dependence of the responsivity. d) Photoresponse spectrum. The gray curve was collected with the near infrared optics set in the FTIR and the black curve with the mid-infrared optics set. The dashed line indicates the measurement noise level at ≈50 counts.

is expected to be nonlinear. Such behavior is intrinsic to systems exhibiting phase transitions, but may not necessarily be desirable for bolometric applications, where stability over large temperature ranges is more customarily sought after. It is possible, however, that the benefits brought about by the greatly enhanced TCR may encourage applications in less conventional bolometric sensing setups that may take advantage of this nonlinearity, such as threshold-based sensing and possibly heterodyne mixing.

The time dependence of the voltage drop across the bolometer as an illuminating infrared LED was tuned on and off by a square wave is shown in **Figure 3**a. The measurement was performed at 40 °C. The decay of the bolometer voltage as the LED is turned on is magnified in Figure 3b. The exponential decay fit, shown in the dashed line, yielded $\tau \approx 83$ ms. The responsivity of the system at 40 °C was found to be ≈48 V/W at 1Hz modulation. Figure 3c shows the behavior of the responsivity as a function of the modulation frequency. The observed decay in responsivity with increasing frequency is consistent with the value of τ measured in Figure 3b. Figure 3d shows infrared photoresponse spectra (measured at 21 °C and ≈55% relative humidity). Photoresponse signal was observed throughout the entire range of our spectrometer (≈1–20 μm).

The temperature dependence of other key bolometric parameters is shown in **Figure 4**a. As the temperature approached the dew point (indicated by the dashed line), the responsivity increased considerably compared with its dehydrated value, and ultimately reached an enhancement factor of almost four compared to the value at 40 °C. The enhancement in the responsivity was intermediate between that of the TCR and the resistance. The time constant (τ) experienced a significant slowdown from 83 ms at 40 °C to over 400 ms at 8 °C. According to Equation 4, the fact that the enhancement in the responsivity (≈3.5×) was considerably less than the product between the enhancements of the TCR and resistance (≈22×) indicates that a potentially substantial decrease in R_{Th} also occurred as a function of the VPT.

Figure 4b shows the relative humidity dependence of the bolometric parameters. The responsivity was observed to increase with the relative humidity up to the dew point. The observed enhancements in the responsivity and TCR with relative humidity are also considerably greater than the enhancement in the resistance, which suggests that the most significant contribution to the responsivity comes from the large TCR observed in this material. Here too, the enhancement in the responsivity was intermediate between those of the TCR and the resistance, suggesting that R_{th} was also affected by the VPT.

The dependence of the photoresponse on the TCR and the relatively large τ in the order of tens to hundreds of milliseconds suggest that the photoresponses observed here are bolometric.[4] Collins[27] showed that oxygen adsorption onto CNTs may lead to large changes in the CNT resistance. For CNT bolometeric systems operating at atmosphere, it is in principle possible that adsorption/desorption of oxygen might occur during the bolometric operation cycles. Collins also observed, however, that significant desorption (enough to appreciably change the resistance of the CNTs) occurred only over long periods of time (≈1 h) and at elevated temperatures (≈150 °C). In our devices, we estimate that the nanocomposite temperature was raised only by a couple of degrees within a detection cycle. Such small changes would not generate appreciable adsorption/desorption. Additionally, oxygen desorption has been found to increase the electrical resistance of CNTs (and adsorption to reduce it).[27] If present in this system, such a mechanism would lead to positive TCR instead of the negative one observed.

3. Conclusion

In summary, a material with giant TCR was achieved in a nanocomposite of CNTs with a phase-change polymer. These nanocomposites incorporate a novel strategy for enhancing the TCR in nanocomposites by introducing large dynamic changes into the contact resistances of a network of randomly dispersed conductive particles. Other temperature sensitive polymers, especially ones exhibiting phase or glass transitions leading to changes in volume and permittivity may be explored in the same

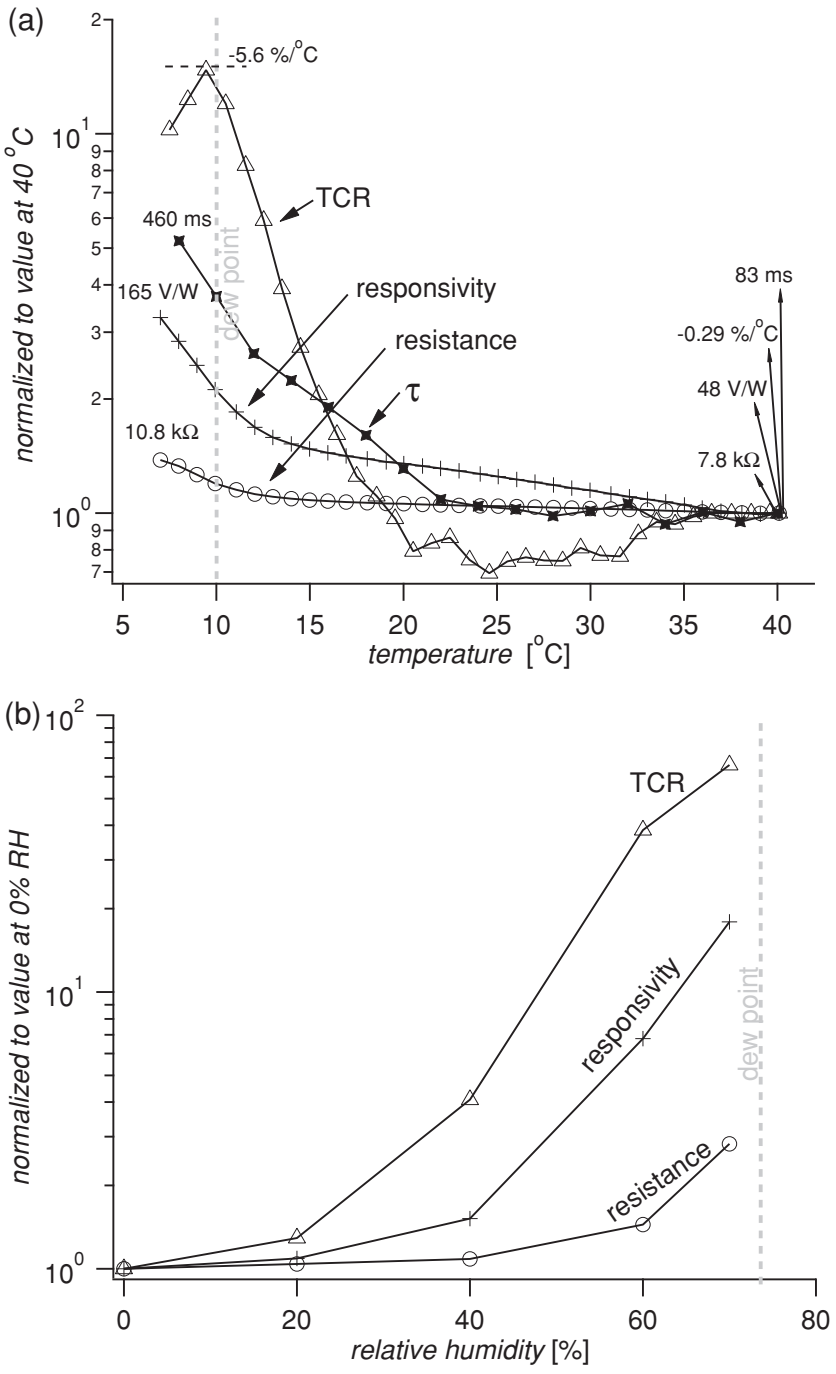

Figure 4. a) Temperature behavior of the responsivity, resistance, TCR, and time constant measured at 60% relative humidity. b) Humidity dependence of the responsivity, resistance and TCR measured at 15 °C.

context. Although a significant enhancement in the bolometric responsivity was achieved as a result of the enhanced TCR, the bolometric time constant also increased dramatically. The increase in the time constant appears to result from the hydration of the nanocomposite. As such, other polymers or solvents having smaller thermal mass than water should be investigated and could lead to enhanced responsivity without a large penalty in the time constant. We note, in addition, that the devices studied in this work were handmade and intended as proof-of-principle. They did not include any sophistication in terms of microbolometer device design and engineering, which are undoubtedly necessary to achieve high performances.[28] We believe that with such design considerations the bolometric performance of this material could be significantly improved.

4. Experimental Section

CNT-PNIPAm Composite Synthesis: Thin-film samples of CNT-PNIPAM composite were prepared by filtration of an aqueous solution of CNTs (Nano-Integris) through a porous alumina filter (Anodisk, Whatman, 20 nm mean pore diameter). The water-dispersed CNTs contained 1% sodium dodecyl sulfate (SDS). An aqueous solution of PNIPAM (molecular weight 74 000 g mol^{-1}, Sigma-Aldrich) containing 1% SDS (Sigma-Aldrich) was then filtered through the same filter. This method resulted in highly uniform nanocomposite films without any observable bundling of CNTs or aggregations of polymer. Measurements were made on as-prepared samples having a CNT mass fraction of 0.05, using the alumina filter as substrate. Contacts were made by attaching wires directly to the films with silver paste.

TCR Measurement: Resistances were measured in a sealed environmental chamber kept at room temperature (≈22 °C) and 1 atm. The relative humidity value inside the measurement chamber was controlled by adjusting the flow of wet and dry N_2 (wet N_2 was obtained by flowing dry N_2 through a water bubbler) and monitored with a hygrometer. The samples were mounted on a thermoelectric heater/cooler plate inside the chamber. The sample temperature was controlled via a temperature controller (LDC 3722B, ILX Lightwave) and monitored by a thermocouple that was mounted onto the Al block that served as sample stage in the chamber. Resistance measurements were taken at sample temperatures between 2 and 45 °C in increments of 1 °C. A source measure unit (Keithley 236, Keithley) was used for the electrical measurements in two point probe mode. Comparative 4-point-probe measurements were also done using a semiconductor parameter analyzer (HP 4145B, Hewlett Packard). Our testing revealed that both four and two-point probe methods yielded similar results, indicating that contact resistances were negligible. The TCR (in%/°C) was calculated from the measured resistance data according to equation (5)

$$\frac{TCR}{(\%/^{\circ}C)} = \frac{100}{R}\frac{\Delta R}{\Delta T} \quad (5)$$

Photoresponse Measurement: A small piece (≈0.5 mm × 1 mm) of sample (including substrate) was suspended across an air gap of ≈0.3 mm between two copper blocks and electrically contacted to the blocks with silver paste. The porosity of the alumina substrate provided some added thermal isolation to the films while maintaining high

structural integrity. The photoresponse was measured by applying a constant current and measuring the voltage drop across the films with either with a lock-in amplifier (Stanford Research, SRS830) or directly with an oscilloscope. Illumination was provided by an infrared light emitting diode (LED, wavelength 880 nm) with a peak power density of 6 mW/cm^2. The measurements were performed at room pressure with the atmosphere in the environmental chamber kept at a constant temperature of ≈20 °C. The sample temperature was controlled independently with a thermoelectric block.

Infrared Spectral Photoresponse Measurement: Measurements were performed with a Fourier transform IR (FTIR) spectrometer (Equinox 55, Bruker) in step-scan mode. Amplitude modulation at 22 Hz was used in the measurements. The FTIR spectrometer uses two interchangeable optics sets (sources and beam splitters) to cover the range of wavelengths from 1–20 μm. For the measurements, the suspended bolometer samples were connected to a Wheatstone bridge circuit. The bridge voltage was amplified with an instrumentation amplifier (LT1167, Linear Technology), the output of which was connected directly to the external detector port of the FTIR. The obtained spectra were then normalized to the signal obtained from a thermopile detector with flat response over the measured range (818P-001-12, Newport).

Supporting Information

Supporting Information is available from the Wiley Online Library or from the author.

Acknowledgements

We gratefully acknowledge support from AFOSR, ARO, DARPA (through Magnolia Optical Technologies Inc.), and the WCU program of Seoul National University.

Received: January 18, 2013
Published online: April 5, 2013

[1] a) M. S. Dresselhaus, G. Dresselhaus, P. Avouris, *Carbon Nanotubes: Synthesis, Structure, Properties, and Applications*, Springer, Berlin, New York **2001**; b) N. Sinha, J. Z. Ma, J. T. W. Yeow, *J. Nanosci. Nanotechnol.* **2006**, *6*, 573.

[2] a) R. C. Jones, *J. Opt. Soc. Am.* **1953**, *43*, 1; b) P. L. Richards, *J. Appl. Phys.* **1994**, *76*, 1.

[3] a) A. E. Aliev, *Infrared Phys. Technol.* **2008**, *51*, 541; b) R. T. Lu, Z. Z. Li, G. W. Xu, J. Z. Wu, *Appl. Phys. Lett.* **2009**, *94*, 163110.

[4] M. E. Itkis, F. Borondics, A. P. Yu, R. C. Haddon, *Science* **2006**, *312*, 413.

[5] P. Merel, J. B. A. Kpetsu, C. Koechlin, S. Maine, R. Haidar, J. L. Pelouard, A. Sarkissian, M. I. Ionescu, X. L. Sun, P. Laou, S. Paradis, *Comptes Rend. Phys* **2010**, *11*, 375.

[6] M. Tarasov, J. Svensson, L. Kuzmin, E. E. B. Campbell, *Appl. Phys. Lett.* **2007**, *90*, 163503.

[7] A. Y. Glamazda, V. A. Karachevtsev, W. B. Euler, I. A. Levitsky, *Adv. Funct. Mater.* **2012**, *22*, 2177.

[8] Z. C. Wu, Z. H. Chen, X. Du, J. M. Logan, J. Sippel, M. Nikolou, K. Kamaras, J. R. Reynolds, D. B. Tanner, A. F. Hebard, A. G. Rinzler, *Science* **2004**, *305*, 1273.

[9] E. S. Snow, J. P. Novak, P. M. Campbell, D. Park, *Appl. Phys. Lett.* **2003**, *82*, 2145.

[10] L. J. Hall, V. R. Coluci, D. S. Galvao, M. E. Kozlov, M. Zhang, S. O. Dantas, R. H. Baughman, *Science* **2008**, *320*, 504.

[11] H. Dai, *Acc. Chem. Res.* **2002**, *35*, 1035.

[12] M. B. Jakubinek, M. A. White, M. F. Mu, K. I. Winey, *Appl. Phys. Lett.* **2010**, *96*, 083105.

[13] F. Niklaus, C. Vieider, H. Jakobsen, *Proc. SPIE* **2007**, 68360D.

[14] P. W. Kruse, *Uncooled Thermal Imaging : Arrays, Systems, and Applications*, SPIE Press, Bellingham, USA **2001**.

[15] D. H. Zhang, K. Ryu, X. L. Liu, E. Polikarpov, J. Ly, M. E. Tompson, C. W. Zhou, *Nano Lett.* **2006**, *6*, 1880.

[16] a) S. Banerjee, D. Chakravorty, *J. Appl. Phys.* **1998**, *84*, 1149; b) A. L. Efros, B. I. Shklovskii, *J. Phys. C: Solid State Phys.* **1975**, *8*, L49; c) N. F. Mott, *Conduction in Non-Crystalline Materials*, Clarendon Press, New York **1987**.

[17] Y. G. Ma, H. J. Liu, C. K. Ong, *Europhys. Lett.* **2006**, *76*, 1144.

[18] D. S. Mclachlan, *J. Appl. Phys.* **1990**, *68*, 195.

[19] H. S. Peng, *J. Am. Chem. Soc.* **2008**, *130*, 42.

[20] P. Sheng, B. Abeles, Y. Arie, *Phys. Rev. Lett.* **1973**, *31*, 44.

[21] M. Heskins, J. E. Guillet, *J. Macromol. Sci., Chem.* **1968**, *A2*, 1441.

[22] H. G. Schild, *Prog. Polym. Sci.* **1992**, *17*, 163.

[23] K. Takahashi, T. Takigawa, T. Masuda, *J. Chem. Phys.* **2004**, *120*, 2972.

[24] a) I. J. Suarez, A. Fernandez-Nieves, M. Marquez, *J. Phys. Chem. B* **2006**, *110*, 25729; b) F. M. Winnik, M. F. Ottaviani, S. H. Bossmann, M. Garciagaribay, N. J. Turro, *Macromolecules* **1992**, *25*, 6007.

[25] K. Iwai, K. Hanasaki, M. Yamamoto, *J. Lumin.* **2000**, *87–9*, 1289.

[26] E. D. Minot, Y. Yaish, V. Sazonova, J. Y. Park, M. Brink, P. L. McEuen, *Phys. Rev. Lett.* **2003**,90, 156401.

[27] P. G. Collins, K. Bradley, M. Ishigami, A. Zettl, *Science* **2000**, *287*, 1801.

[28] J. Piotrowski, A. Rogalski, *High-Operating-Temperature Infrared Photodetectors*, SPIE Press, Bellingham, USA **2007**.